

**Production of the C4 ligands.** The C4 IgG heavy and light chains were cloned into the AbVec2.0-IGHG1 and AbVec1.1-IGLC plasmids, respectively (16). For the Fab C4, the IgG Fc fragment was replaced by a polyhistidine (6xHIS) tag in the heavy chain plasmid. Human HEK293 Freestyle cells (Thermo-Fisher) ( $2.5 \times 10^6$  cells/mL) were transiently co-transfected in 100 mL of Freestyle medium (Thermo-Fisher), by adding 150  $\mu$ g of each recombinant plasmid and 1.8 mL of linear polyethylenimine (0.5 mg/mL, Polysciences). Transfected cells were incubated for 7 days at 37°C and 120 rpm, in a humidified atmosphere with 8% CO<sub>2</sub>. The culture supernatant containing the secreted C4 ligands was purified using HiTrap Protein A, Lambda FabSelect or HisTrap Excel columns (GE Healthcare) for IgG C4, IgG C4 (H310A/H435Q) and Fab C4, respectively. A final size-exclusion chromatography was performed using Sephacryl-S-200 HR columns (Sigma) with PBS. Purity of the C4 ligand solutions was evaluated by sodium dodecyl sulfate polyacrylamide gel electrophoresis (SDS-PAGE).

**Bio-layer interferometry.** Binding kinetics of the C4 ligands to human PD-L1 (Sinobiological) were determined by bio-layer interferometry, using an Octet RED96 instrument (ForteBio). Anti-hIgG Fc Capture Biosensors (ForteBio) were loaded with the IgG C4 or with the IgG C4 (H310A/H435Q) (50 nM) for 60 s. Association between the C4 IgGs and human PD-L1 was measured at different PD-L1 concentrations (1.6 nM–100 nM) for 300 s, before dissociation for 1000 s in kinetic buffer (PBS with 0.5% BSA and 0.05% Tween 20). Streptavidin Biosensors (ForteBio) were loaded with biotinylated human PD-L1 (50 nM) for 60 s. Association between the Fab C4 and human PD-L1 was measured at different Fab concentrations (0.78 nM–6.3 nM) for 200 s, before dissociation for 1000 s in kinetic buffer. After baseline subtraction, binding curves were fitted to a global 1:1 binding model to calculate the different kinetic constants ( $k_a$ ,  $k_d$ ,  $K_D$ ).

**Radiolabeling of the C4 ligands with <sup>89</sup>Zr.** The C4 ligands were covalently conjugated with the chelator p-isothiocyanatobenzylferrioxamine (p-NCS-Bz-DFO, MacroCyclics) on random lysine residues. Radiolabeling with <sup>89</sup>Zr (PerkinElmer) was performed according to a previously published protocol (17). 1 mL of C4 ligand solution (5 mg/mL in PBS) was adjusted to pH 9.3 with sodium carbonate (Na<sub>2</sub>CO<sub>3</sub>, 0.1 M). A 4-fold molar excess of p-NCS-Bz-DFO (10 mM in DMSO) was added dropwise to the C4 ligand solution with rigorous mixing (500 rpm). The reaction mixture was then gently mixed (350 rpm) for 45 min at 37°C. The DFO-C4 ligand conjugates were subsequently purified with a PD-10 column (GE Healthcare), using a gentisic acid solution (5 mg/mL in 0.25 M sodium acetate, pH 5.4–5.6) as the mobile phase. 200  $\mu$ L of [<sup>89</sup>Zr]Zr-oxalic acid solution (1 M) were neutralized with 90  $\mu$ L of Na<sub>2</sub>CO<sub>3</sub> (2 M). 500  $\mu$ L of DFO-C4 ligand solution (2.5 mg/mL) were then incubated with <sup>89</sup>Zr (111 MBq) for 1 h at 37°C. The reaction mixture was adjusted to pH 7.2 with HEPES (1 M, pH 7.1–7.3). The <sup>89</sup>Zr-labeled DFO-C4 ligand conjugates were first purified with a PD-10 column using a gentisic acid solution as the mobile phase, before being further concentrated and buffer exchanged in HEPES (0.5 M, pH 7.1–7.3) with a Vivaspin centrifugal concentrator (Sartorius). Radiochemical purity of the <sup>89</sup>Zr-DFO-C4 solution was assessed by instant thin layer chromatography (iTLC) and size-exclusion high-performance liquid chromatography (SE-HPLC). iTLC was performed on iTLC-SG glass microfiber papers impregnated with silica gel (Agilent Technologies) as the stationary phase, using a citric acid solution with 5% acetonitrile (20 mM, pH 4.9–5.1) as the mobile phase. The iTLC papers were read in a Mini-Scan TLC Imaging Scanner (Eckert & Ziegler). SE-HPLC was performed using a DIONEX System (Thermo-Fisher) with a bioZen 1.8  $\mu$ m SEC-2 LC column (Phenomenex). A linear-gradient elution was carried out with a solution of KH<sub>2</sub>PO<sub>4</sub> (50 mM) and KCl (250 mM) (pH 6.8), at a flow rate of 0.2 mL/min. Eluted species were detected with a UV detector (UVD 170U UV/VIS) and a scintillation detector (Packard).

**Cell culture.** The human NSCLC cell lines H1975 (ATCC CRL-5908) and A549 (ATCC CCL-185) were purchased from the American Type Culture Collection (ATCC). Cells were cultured in RPMI-1640 medium with GlutaMAX (Gibco) for the H1975 cell line or Dulbecco's Modified Eagle's medium with GlutaMAX (Gibco) for the A549 cell line, supplemented with 10% fetal bovine serum (Gibco) and 1% antibiotic-antimycotic solution (Gibco), at 37°C in a humidified atmosphere with 5% CO<sub>2</sub>. Cell lines were regularly tested negative for mycoplasma contamination with the MycoAlert Mycoplasma Detection Kit (Lonza). Low-passage (P20–P25) cell cultures were used for all experiments.

**Cell binding assays.** H1975 cells were harvested in their exponential phase of growth and resuspended in RPMI culture medium (Gibco) with 1% BSA (Thermo-Fisher) at a concentration of 8 million cells/mL. 250  $\mu$ L of cell solution (2 million cells) were mixed with 250  $\mu$ L of <sup>89</sup>Zr-IgG C4, <sup>89</sup>Zr-IgG C4 (H310A/H435Q) or <sup>89</sup>Zr-Fab C4 (2 pmol, 4–8  $\mu$ Ci) in HEPES buffer. For each C4 radioligand, a blocking experiment was also performed by mixing 250  $\mu$ L of cell solution

with 250  $\mu\text{L}$  of C4 radioligand (2 pmol) and 100X molar excess of non-radiolabeled C4 ligand in HEPES buffer. The reaction mixture was incubated for 2 h at 37°C. Cells were then washed 3 times with cold PBS and cell-associated activity was measured with the Wizard<sup>2</sup> gamma counter (PerkinElmer). Cell-associated activity was expressed as percentage of the total activity added per sample. Each condition was performed in N = 6 replicates.

**Immunoblotting.** PD-L1 expression in human NSCLC cell lines was evaluated by Western blot analysis. Total protein concentration in cell lysates was determined by a BCA protein assay kit (Sigma-Aldrich). Equal amounts (30  $\mu\text{g}$ ) of total proteins were separated by SDS-PAGE on 4-15% Mini-PROTEAN TGX gels (Bio-Rad) and transferred over to a polyvinylidene fluoride (PVDF) membrane by semi-dry blotting. After transfer, blots were blocked for 2 h at RT with 5% BSA (Thermo-Fisher) and incubated overnight at 4°C with the following primary antibodies: rabbit anti-human PD-L1 (1:1000, clone E1L3N, Cell Signaling #13684) and rabbit anti-human  $\alpha$ -tubulin (1:1000, Cell Signaling #2144). Blots were then incubated for 1 h at RT with an HRP-conjugated donkey anti-rabbit secondary antibody (1:10,000, Jackson ImmunoResearch 711-035-152). Proteins were detected using the Clarity Western ECL Substrate (Bio-Rad). Immunoblots were imaged with the FUSION FX imaging system (Vilber). Image post-processing (cropping, global contrast adjustment) was performed with ImageJ (v1.53i).

**Animals.** Female nude mice (*Mus musculus*, NMRI-FOXN1 Nu/Nu, Janvier, 10  $\pm$  1 weeks, 27.8  $\pm$  1.4 g) were used for the PET imaging studies. Animal experiments were performed according to the European Directive 2010/63/EU on the protection of laboratory animals and to its transposition into the French law (Decree No. 2013-118). The research project was conducted at the CEA-SHFJ imaging platform (authorization D91-471-105) and was approved by a local ethics committee (CETEA-CEA DSV IdF). Mice were housed in individually-ventilated cages in a temperature (22°C) and humidity (40%)-controlled room, with a 12-h light/12-h dark cycle. Animal experiments (subcutaneous injection of tumor cells, PET imaging) were performed under anesthesia with isoflurane in oxygen (3% for induction and 1.5–2% for maintenance) at 1.5 L.min<sup>-1</sup>. The body temperature of anesthetized mice was maintained at 37°C using heating pads.

**Subcutaneous injection of tumor cells.** Anesthetized mice were subcutaneously inoculated in both lower flanks with H1975 or A549 cells (4-5  $\times$  10<sup>6</sup> cells) suspended in PBS/Matrigel (BD Biosciences) (1:1). Subcutaneous tumor size and animal weight were measured two times per week. Mice were used for PET imaging studies when tumors reached  $\sim$ 8 mm at the largest diameter.

#### **microPET/CT imaging.**

**Radioligand injection.** Tumor-bearing mice received an intravenous bolus injection of <sup>89</sup>Zr-labeled C4 ligand in HEPES ( $\sim$ 100  $\mu\text{L}$ , 3.7  $\pm$  0.7 MBq, 7.0  $\pm$  3.0 MBq/nmol, 0.6  $\pm$  0.3 nmol) via a catheter placed in the lateral tail vein. For blocking studies, mice were co-injected with a 20X molar excess of non-radiolabeled C4 ligand ( $\sim$ 200  $\mu\text{L}$ , 1.2 nmol).

**PET/CT acquisition.** Whole-body PET emission scans were performed using an Inveon microPET scanner and an Inveon microPET/CT scanner (Siemens), with an axial field of view of 12.7 cm and a spatial resolution of  $\sim$ 1.5 mm full width half-maximum. A 350–650 keV energy window and a 3.43 ns timing window were used for data acquisition. A 60-min dynamic PET scan was performed immediately after injection of the C4 radioligand. 20-min static PET scans were subsequently acquired at selected times (4 h, 24 h, 48 h, 72 h and 7 days) post-injection (p.i.). For the Inveon microPET scanner, after each PET emission scan, a 6.6-min transmission scan using two rotating cobalt-57 (<sup>57</sup>Co) point sources (120-125 keV energy window) was recorded for photon attenuation correction. For the Inveon microPET/CT scanner, after each PET emission scan, a 11-min CT scan (120 projections, 220 total gantry rotations) was performed for photon attenuation correction and anatomical co-registration.

**PET/CT image reconstruction.** PET images were reconstructed with the Inveon Acquisition Workspace software (v2.1) using a three-dimensional ordinary Poisson ordered-subset expectation maximization followed by maximum *a posteriori* algorithm (OP-OSEM3D-MAP) (2 OSEM3D iterations, 18 MAP iterations with 16 MAP subsets). The size of the image matrix was 256  $\times$  256 pixels with 159 slices, resulting in a voxel size of 0.38  $\times$  0.38  $\times$  0.80 mm. Normalization as well as corrections for dead-time, scatter, decay and attenuation were applied to all PET data. Dynamic PET images were arranged into 24 frames ranging from 0.5 to 5 min each (3  $\times$  0.5 min, 5  $\times$  1 min, 5  $\times$  2 min, 3  $\times$  3 min, 3  $\times$  4 min, 4  $\times$  5 min and 1  $\times$  2.5 min). CT images were reconstructed using a Feldkamp cone beam reconstruction algorithm, with a cubic voxel size of 0.21 mm<sup>3</sup> in a 496  $\times$  496  $\times$  630 matrix.

**PET/CT image analysis.** Image analysis was performed with the PMOD software (v3.9). Volumes of interest (VOIs) were defined in main organs and tumor based on both CT (when available) and PET images. Fixed-size spherical VOIs (3.5-8 mm<sup>3</sup>) were drawn in representative parts of the heart, liver and kidneys. Mouse whole-body, spleen and subcutaneous tumors were delineated semi-automatically, with the help of the auto iso-contour tool. To quantify C4 radioligand uptake, the mean activity concentration (kBq/cm<sup>3</sup>) in each VOI was decay-corrected to the injection time and divided by the total injected activity (kBq) to obtain the percentage of injected dose per volume of tissue (%ID/cm<sup>3</sup>).

**Ex vivo biodistribution.** Immediately after the last PET imaging session, mice were sacrificed by cervical dislocation. Blood and major organs (brain, heart, lung, liver, kidney, spleen, intestine, tumor, muscle, bone) were collected, weighed, and counted with a Wizard<sup>2</sup> gamma counter (PerkinElmer). Radioactivity data (kBq) were background-corrected, decay-corrected to injection time and divided by the total injected activity (kBq) and the organ weight (g), to obtain the percentage injected dose per gram of tissue (%ID/g). Supplemental Figure 3.

**Immunohistochemistry.** PD-L1 expression in NSCLC xenografts was evaluated *ex vivo* by immunohistochemistry (IHC). Excised tumors were snap-frozen and stored at -80°C until processing. Frozen tumors were cryo-sectioned into 12-µm thick slices. Frozen tumor sections were fixed for 10 min at RT in 10% neutral-buffered formalin solution (Sigma-Aldrich). Non-specific binding sites were blocked by incubation for 2 h at RT with 10% FBS (Gibco) and 1% bovine serum albumin (BSA) (Thermo-Fisher). After blocking, slides were incubated overnight at 4°C with a rabbit anti-human PD-L1 primary antibody (1:100, clone E1L3N, Cell Signaling #13684). Slides were then rinsed and incubated for 1 h at RT with an HRP-conjugated donkey anti-rabbit secondary antibody (1:500, Jackson ImmunoResearch 711-035-152). Peroxidase activity was detected by incubating slides for 30 min at RT with 3-3'-diaminobenzidine (DAB) (BD Pharmingen). Tumor sections were subsequently counterstained with Harris hematoxylin (Sigma-Aldrich). Slides were eventually mounted with the Eukitt Quick-hardening mounting medium (Fluka Analytical). Standard hematoxylin and eosin (H&E) staining was also performed on adjacent tumor sections, using Harris hematoxylin and Eosin Y alcoholic (Sigma-Aldrich). Transmitted light images of stained tumor sections were acquired with the Axio Observer 5 microscope (Zeiss) at 20X magnification. Image post-processing (stitching, white balance, global contrast adjustment and addition of scale bar) was performed with the ZEN software (v2.6, Zeiss).

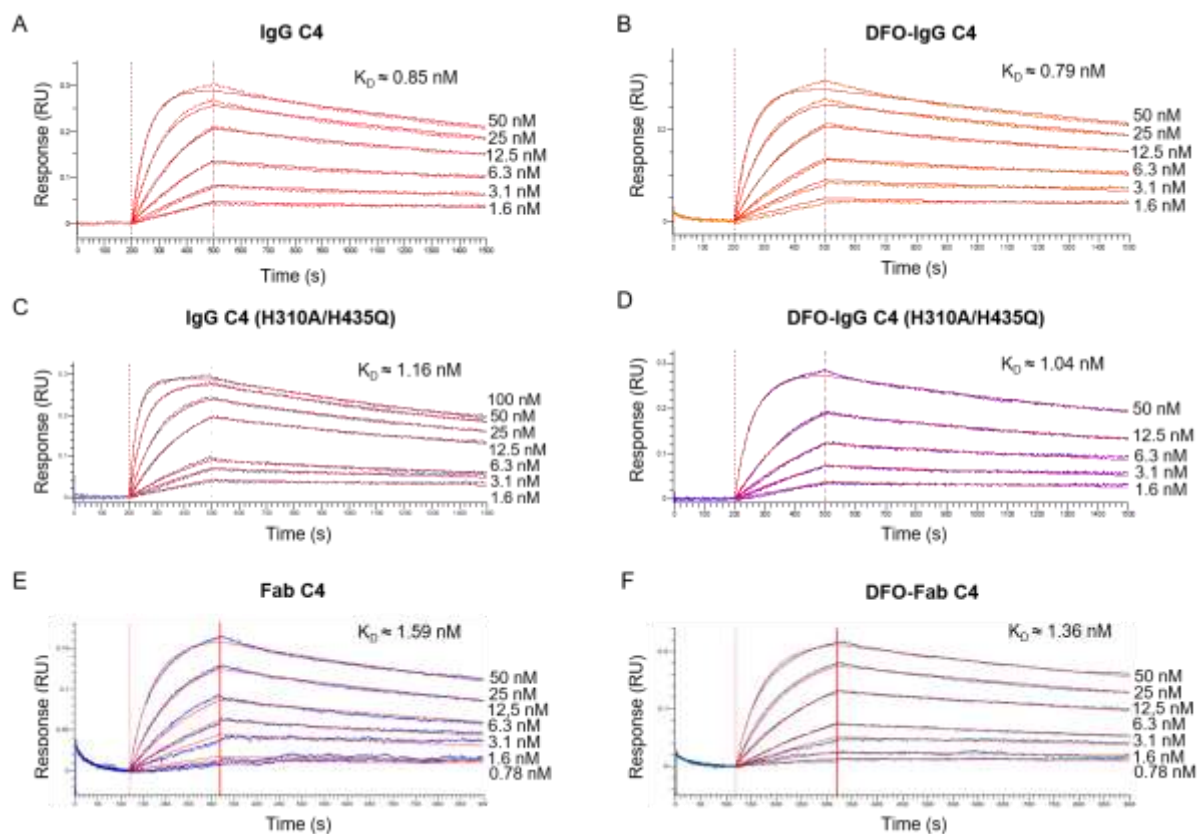
**Flow cytometry.** PD-L1 cell surface expression on human NSCLC cells cultured *in vitro* and on cell suspensions obtained from dissociated human NSCLC xenografts was evaluated by flow cytometry. Immediately after surgical excision, NSCLC tumors were minced into small tissue fragments and incubated in Accutase enzyme cocktail (Sigma-Aldrich) for 1 h at 37°C with regular mixing. Digested tumor tissues were filtered through cell strainers (PluriSelect) of decreasing mesh sizes (500, 200, 70 and 40 µm). Single-cell suspensions (~10<sup>6</sup> cells per sample) were incubated for 20 min on ice with the following fluorescent-labeled antibodies (100 µL, 10 µg/mL) in cell staining buffer (BioLegend): PE-conjugated anti-human PD-L1 antibody (clone 29E.2A3, BioLegend #329706) and PE-conjugated mouse IgG2b, κ isotype control (clone MPC-11, BioLegend #400314). For assessment of cell viability, cells were incubated for 30 min at RT with the Zombie Green viability dye (1:500, BioLegend). After incubation in fluorescent reagents, cells were washed 2 times and resuspended in cell staining buffer. Flow cytometry acquisitions were performed on the Attune NxT Acoustic Focusing Cytometer (Invitrogen). Unstained and single-color compensation controls were used for data compensation. Data analysis was performed with the FlowJo software (v10.7).

**Blood pharmacokinetics.** Plasma activity concentrations of the C4 radioligands were calculated from their image-derived blood pool activity concentrations. Considering that antibodies/antibody fragments do not partition into red blood cells and are restricted to the plasma, a blood-to-plasma concentration ratio of 0.55 was used. For each C4 radioligand, plasma time-activity curves (TACs) of individual mice were pooled together and fitted to a two-compartment model with intravenous bolus input and first-order elimination, using the NONMEM software (v6.2).

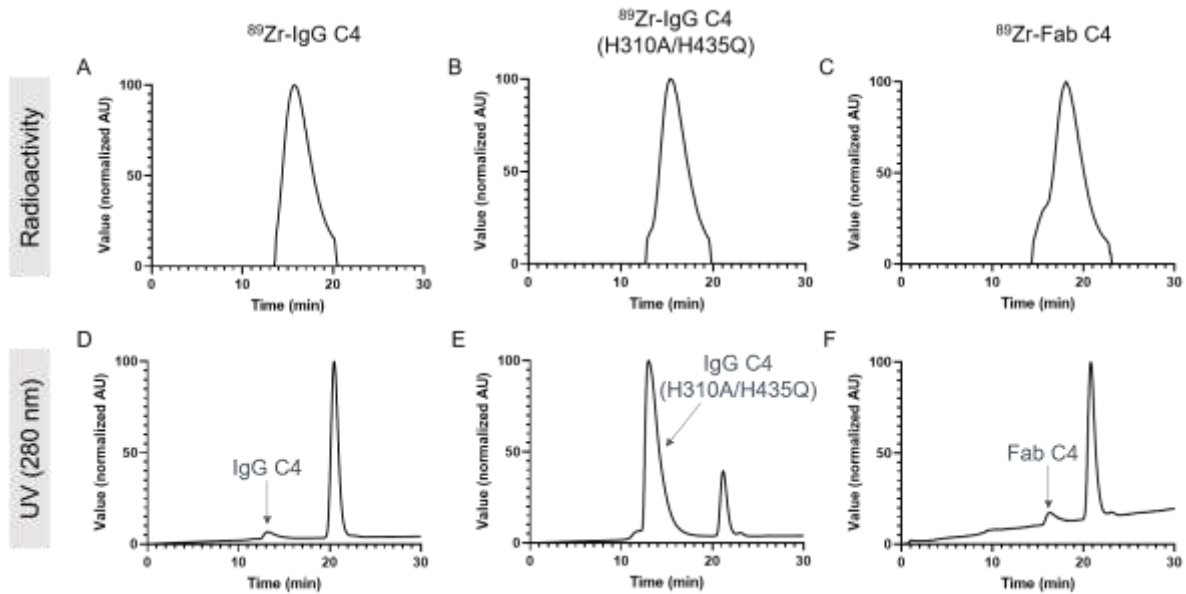
**Dosimetry analysis.** For each C4 radioligand, human organ absorbed dose estimates were extrapolated from longitudinal biodistribution data in mice. For each mouse, non-decay-corrected mean activity concentrations (Bq/cm<sup>3</sup>) in main source organs (blood pool, liver, kidneys, spleen, whole-body) were derived from PET images and multiplied by corresponding organ volumes to obtain the organ mean activities (Bq). Organ mean activities were

plotted against time to obtain the organ TACs. Each organ TAC was numerically integrated (trapezoidal method) over the imaging time-course, and a single exponential decay function with the half-life of  $^{89}\text{Zr}$  was extrapolated and analytically integrated beyond the last imaging time point with the R software (v4.0.4). The organ cumulated activity (Bq/s) was derived as the sum of the numerical and analytical integrations. For each mouse, source organ cumulated activities (Bq/s) were divided by the total administered activity (Bq) to obtain the organ residence times (kBq.h/kBq). The cumulated activity in the remainder of the body was calculated as the difference between the whole-body cumulated activity and the cumulated activities in all other source organs. Murine source organ residence times were used as input in the IDAC-Dose (v2.1) software (18) for calculation of human organ absorbed doses and whole-body effective dose. For the three C4 radioligands, murine organ absorbed doses were also estimated with the Rodent Dose Evaluation Software (RODES) (19).

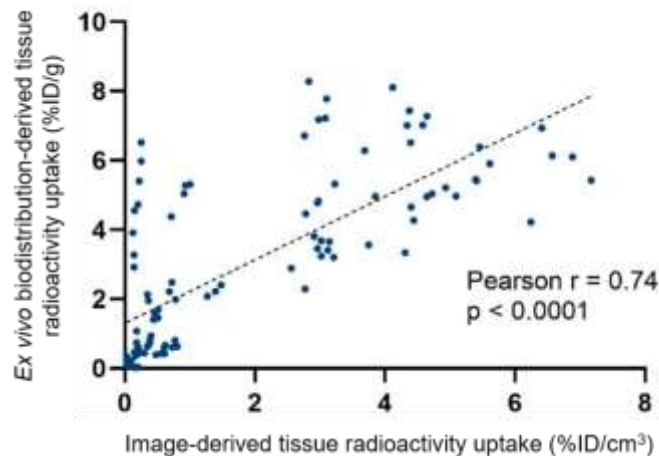
**Statistical analysis.** Statistical analyses were performed with GraphPad Prism (v9.0.1). Unless stated otherwise, data are presented as mean  $\pm$  standard deviation (SD). Two-tailed unpaired or paired Student t tests were used for two-group data comparison (\*  $P < 0.05$ , \*\*  $P < 0.01$ , \*\*\*  $P < 0.001$ , \*\*\*\*  $P < 0.0001$ ).



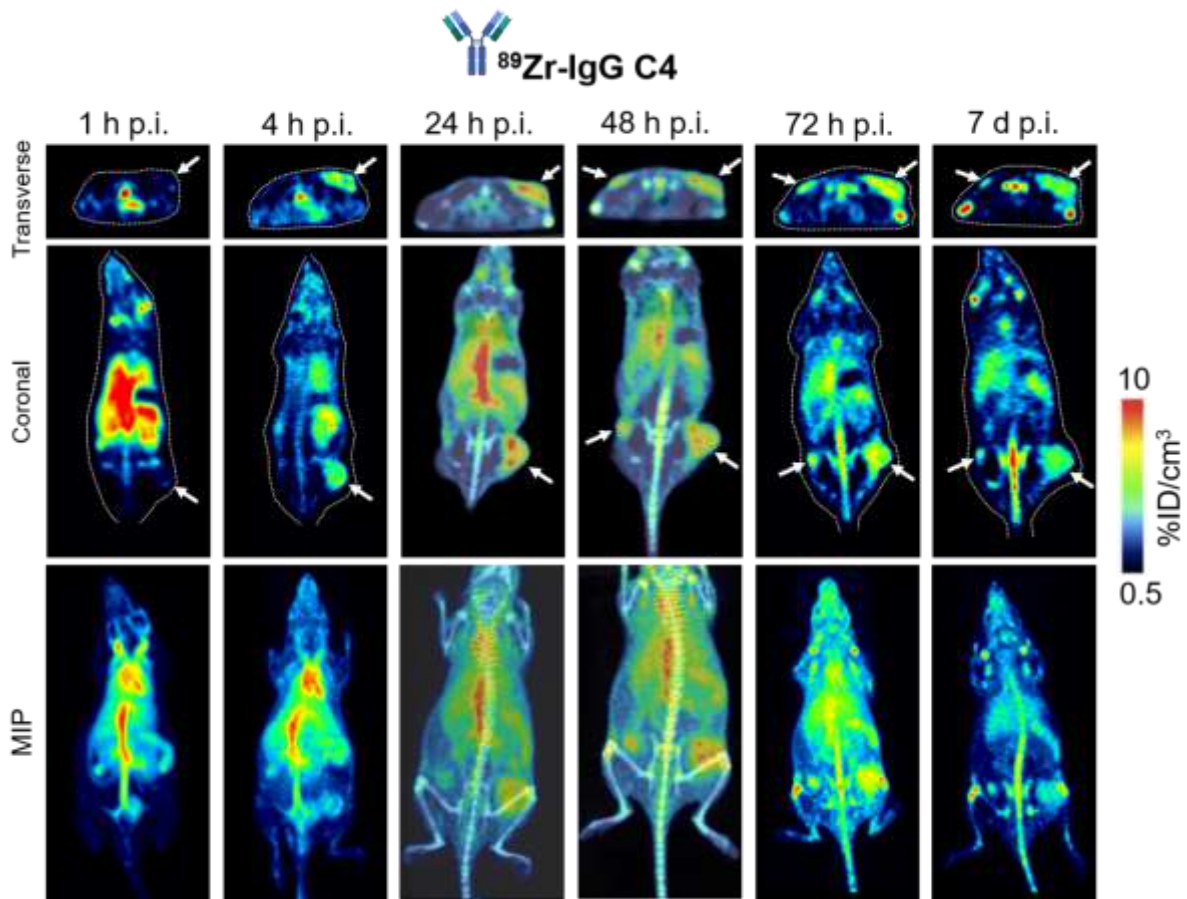
**Supplemental Figure 1. Binding kinetics of the C4 ligands to human PD-L1.** Bio-layer interferometry sensorgrams of binding of IgG C4 (A), DFO-IgG C4 (B), IgG C4 (H310A/H435Q) (C), DFO-IgG C4 (H310A/H435Q) (D), Fab C4 (E) and DFO-Fab C4 (F) to the human PD-L1 protein. Affinity constant ( $K_D$ ) values are indicated. RU: response unit.



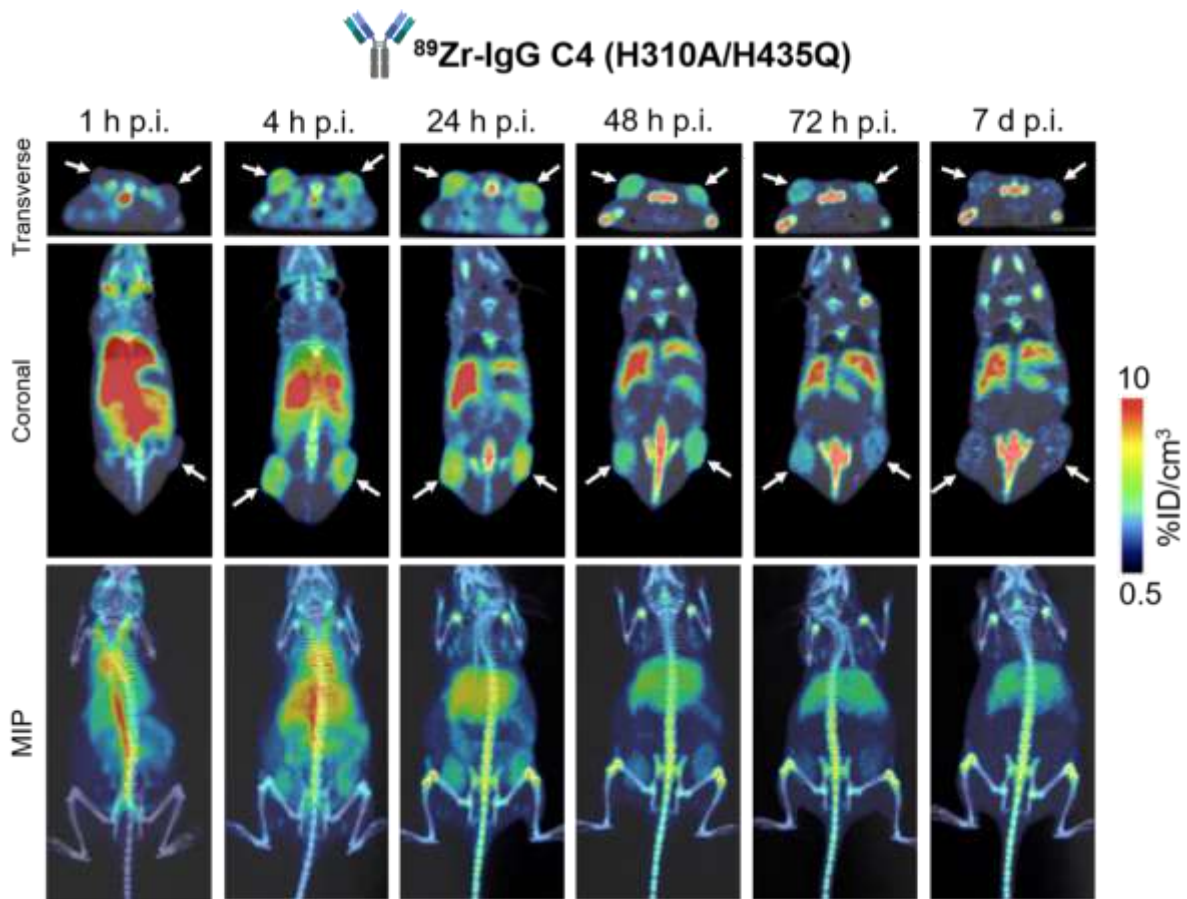
**Supplemental Figure 2. Assessment of radiochemical purity by HPLC after radiolabeling of the C4 ligands with  $^{89}\text{Zr}$ .** Representative HPLC chromatograms of purified  $^{89}\text{Zr}$ -IgG C4 (A and D),  $^{89}\text{Zr}$ -IgG C4 (H310A/H435Q) (B and E) and  $^{89}\text{Zr}$ -Fab C4 (C and F), with radioactivity detection (A, B and C) and UV detection at 280 nm (D, E, and F). The second peak observed at ~22 min on the UV chromatograms corresponds to the gentisic acid still remaining in the purified C4 radioligand solutions. AU: arbitrary unit, UV: ultraviolet.



**Supplemental Figure 3. Correlation between quantification of C4 radioligand tissue uptake by *ex vivo* biodistribution and by PET image analysis.** Tissue uptake values of the C4 radioligands derived from *ex vivo* biodistribution (heart, liver, kidneys, spleen, muscle and tumor) strongly correlated with those derived from analysis of PET images at the last imaging time-point (Pearson  $r = 0.74$ ,  $p < 0.0001$ ). Data from PET imaging experiments on H1975 tumor-bearing mice with the  $^{89}\text{Zr}$ -labeled IgG C4, IgG C4 (H310A/H435Q) and Fab C4, with or without blocking, were pooled ( $N = 6$  experiments). For the  $^{89}\text{Zr}$ -Fab C4, kidneys were excluded from the analysis as the *ex vivo* kidney counting gave values superior to 200 %ID/g. %ID/cm<sup>3</sup>: percentage injected dose per volume of tissue, %ID/g : percentage injected dose per gram of tissue.

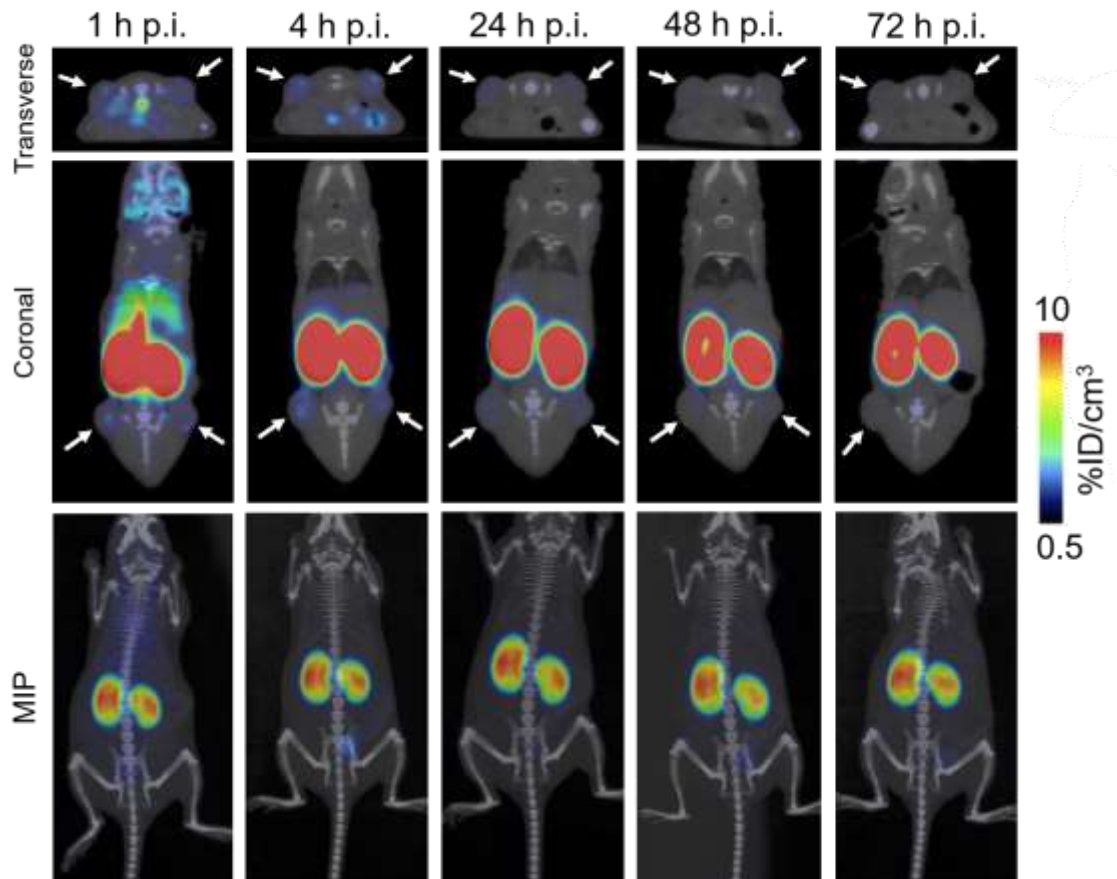


**Supplemental Figure 4. Longitudinal microPET/CT imaging with the anti-PD-L1 <sup>89</sup>Zr-IgG C4 in a PD-L1<sup>+</sup> human NSCLC xenograft model.** Representative microPET/CT image sections (transverse and coronal) and MIP images of female nude mice bearing subcutaneous PD-L1<sup>+</sup> H1975 xenografts (white arrows), obtained at selected times after <sup>89</sup>Zr-IgG C4 administration. MIP: maximum intensity projection, p.i.: post-injection, %ID/cm<sup>3</sup>: percentage injected dose per volume of tissue.

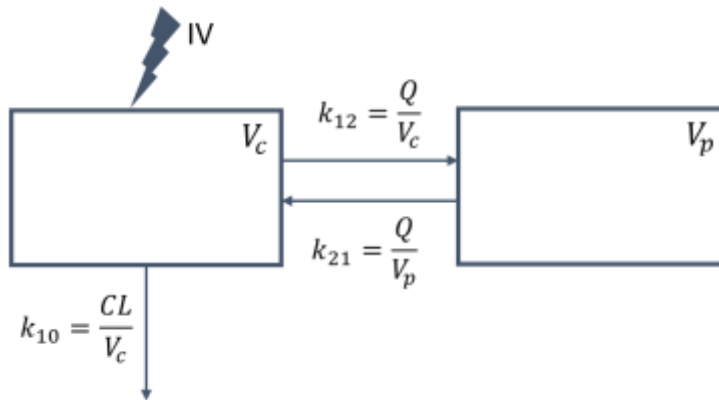


**Supplemental Figure 5. Longitudinal microPET/CT imaging with the anti-PD-L1 <sup>89</sup>Zr-IgG C4 (H310A/H435Q) in a PD-L1<sup>+</sup> human NSCLC xenograft model.** Representative microPET/CT image sections (transverse and coronal) and MIP images of female nude mice bearing subcutaneous PD-L1<sup>+</sup> H1975 xenografts (white arrows), obtained at selected times after <sup>89</sup>Zr-IgG C4 (H310A/H435Q) administration. MIP: maximum intensity projection, p.i.: post-injection, %ID/cm<sup>3</sup>: percentage injected dose per volume of tissue.

## <sup>89</sup>Zr-Fab C4

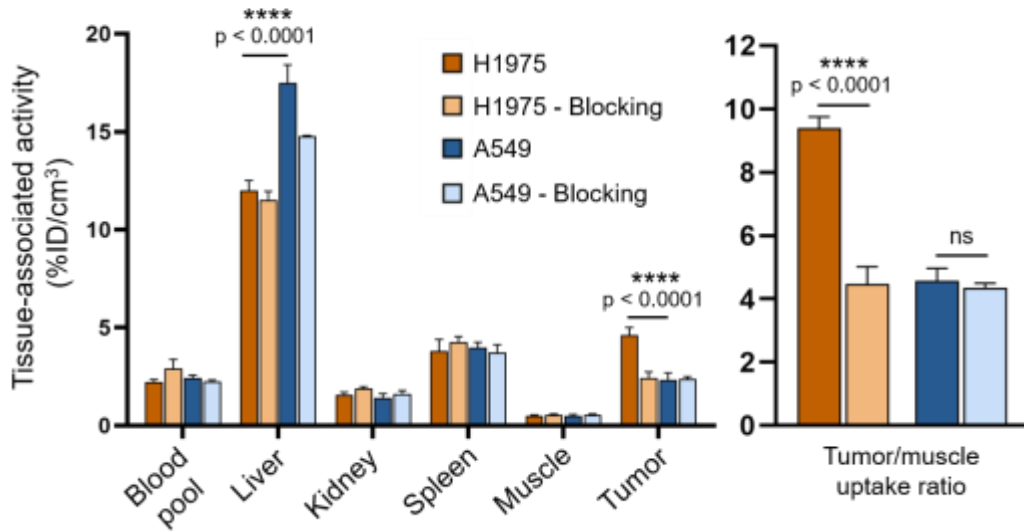


**Supplemental Figure 6. Longitudinal microPET/CT imaging with the anti-PD-L1 <sup>89</sup>Zr-Fab C4 in a PD-L1<sup>+</sup> human NSCLC xenograft model.** Representative microPET/CT image sections (transverse and coronal) and MIP images of female nude mice bearing subcutaneous PD-L1<sup>+</sup> H1975 xenografts (white arrows), obtained at selected times after <sup>89</sup>Zr-Fab C4 administration. MIP: maximum intensity projection, p.i.: post-injection, %ID/cm<sup>3</sup>: percentage injected dose per volume of tissue.

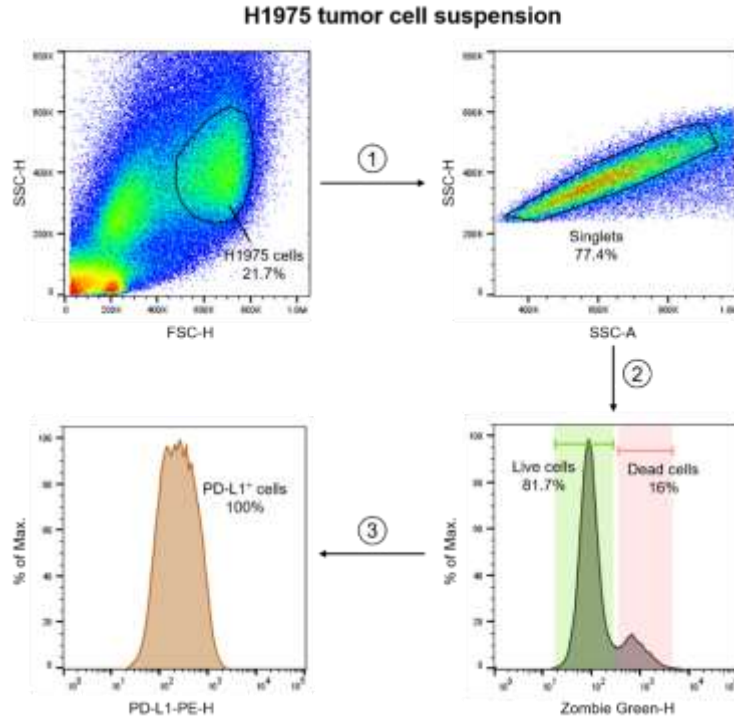


**Supplemental Figure 7. Schematic representation of a two-compartment model with intravenous bolus input and first-order elimination.** This model was used to fit the plasma time-activity curves of H1975 tumor-bearing female nude mice injected with the C4 radioligands. CL: clearance from central compartment, IV: intravenous injection,  $k_{10}$ : elimination rate constant from central compartment,  $k_{12}$ : distribution rate constant from central to peripheral compartment,  $k_{21}$ : distribution rate constant from peripheral to central compartment, Q: clearance from peripheral to central compartment,  $V_c$ : volume of distribution of central compartment,  $V_p$ : volume of distribution of peripheral compartment.

**<sup>89</sup>Zr-IgG C4 (H310A/H435Q)**  
24 h p.i.



**Supplemental Figure 8. PD-L1-specific tumor targeting of the <sup>89</sup>Zr-IgG C4 (H310A/H435Q).** Image-derived *in vivo* biodistribution of the <sup>89</sup>Zr-IgG C4 (H310A/H435Q) in female nude mice bearing subcutaneous PD-L1<sup>+</sup> H1975 xenografts or PD-L1<sup>-</sup> A549 xenografts. For blocking experiments, mice were co-injected with a 20X molar excess of non-radiolabeled IgG C4 (H310A/H435Q). While this blocking dose significantly reduced <sup>89</sup>Zr-IgG C4 (H310A/H435Q) uptake in H1975 xenografts (by ~50%), it did not affect radioligand uptake in A549 xenografts. <sup>89</sup>Zr-IgG C4 (H310A/H435Q) uptake values in non-blocked and blocked A549 tumors were similar to that in blocked H1975 tumors (~2-2.5 %ID/cm<sup>3</sup>). Data are presented as mean ± SD, N = 6 mice/group (no blocking) and N = 3-4 mice/group (blocking). A two-tailed unpaired Student t test was used for two-group data comparison. p.i.: post-injection, %ID/cm<sup>3</sup>: percentage injected dose per volume of tissue.



**Supplemental Figure 9. Gating strategy employed for flow cytometry experiments on single-cell suspensions derived from solid tumors.** Representative plots obtained in a flow cytometry experiment on H1975 tumor cells incubated with the Zombie Green viability dye and a PE-conjugated anti-human PD-L1 antibody. (1) Cells were first gated based on forward scatter (FSC) and side scatter (SSC) characteristics on the SSC-H vs FSC-H density plot. (2) Coincident events that could represent cell clumps were excluded by gating singlets on the SSC-H vs SSC-A density plot. (3) Viable cells were then selected on the Zombie Green-H histogram: the first peak (Zombie Green negative) represented the fraction of viable cells within the sample, whereas the second peak (Zombie Green positive) represented dead cells with compromised membranes permeant to the fluorescent dye. No further gating was performed. For each gate, the percentage of events from the parent gate is indicated. PE: phycoerythrin.

**Supplemental Table 1. Murine dosimetry of the C4 radioligands.** For each C4 radioligand, cumulated activities (Bq/s) in main source organs (blood pool, liver, kidneys, spleen) of individual mice were used as input in the RODES software for calculation of murine organ absorbed doses (mGy). The RODES female mouse phantom (20 g) was selected. For each mouse, estimated absorbed doses were divided by the total administered activity (MBq). Data are presented as mean  $\pm$  SD. Organs with the highest absorbed dose estimates are indicated in bold.

Target organ	Organ absorbed dose estimate (mGy/MBq)		
	<sup>89</sup> Zr-IgG C4 N = 5 mice	<sup>89</sup> Zr-IgG C4 (H310A/H435Q) N = 6 mice	<sup>89</sup> Zr-Fab C4 N = 6 mice
<b>Heart</b>	<b>1.13 <math>\pm</math> 0.10</b>	<b>1.22 <math>\pm</math> 0.04</b>	<b>0.34 <math>\pm</math> 0.07</b>
Lungs	0.18 $\pm$ 0.01	0.25 $\pm$ 0.01	0.06 $\pm$ 0.02
<b>Liver</b>	<b>0.41 <math>\pm</math> 0.01</b>	<b>0.73 <math>\pm</math> 0.04</b>	<b>0.12 <math>\pm</math> 0.01</b>
Stomach	0.05 $\pm$ 0.001	0.08 $\pm$ 0.004	0.05 $\pm$ 0.01
<b>Spleen</b>	<b>0.24 <math>\pm</math> 0.02</b>	0.18 $\pm$ 0.01	0.10 $\pm$ 0.02
<b>Kidneys</b>	0.22 $\pm$ 0.02	<b>0.37 <math>\pm</math> 0.03</b>	<b>1.97 <math>\pm</math> 0.29</b>
Esophagus	0.16 $\pm$ 0.002	0.26 $\pm$ 0.013	0.05 $\pm$ 0.007
Intestines	0.01 $\pm$ 0.001	0.02 $\pm$ 0.001	0.02 $\pm$ 0.004
Colon	0.018 $\pm$ 0.0004	0.03 $\pm$ 0.002	0.05 $\pm$ 0.008
Spinal cord	0.01 $\pm$ 0.0004	0.02 $\pm$ 0.001	0.02 $\pm$ 0.002
Skeleton	0.01 $\pm$ 0.0003	0.02 $\pm$ 0.001	0.01 $\pm$ 0.001
Thyroid	0.004 $\pm$ 0.0002	0.01 $\pm$ 0.0003	0.003 $\pm$ 0.0003
Ovaries	0.01 $\pm$ 0.001	0.03 $\pm$ 0.001	0.09 $\pm$ 0.01
Soft tissues	0.02 $\pm$ 0.001	0.03 $\pm$ 0.002	0.03 $\pm$ 0.003
Whole-body	0.06 $\pm$ 0.001	0.09 $\pm$ 0.004	0.07 $\pm$ 0.01

**Supplemental Table 2. Binding kinetics of the C4 ligands to human PD-L1.** Kinetic constants of C4 ligand binding to human PD-L1 were measured by bio-layer interferometry.

C4 ligand	K <sub>D</sub> (nM)	k <sub>a</sub> (M <sup>-1</sup> .s <sup>-1</sup> )	k <sub>d</sub> (s <sup>-1</sup> )
IgG C4	0.85	3.67 x 10 <sup>5</sup>	3.15 x 10 <sup>-4</sup>
DFO-IgG C4	0.79	3.76 x 10 <sup>5</sup>	2.99 x 10 <sup>-4</sup>
IgG C4 (H310A/H435Q)	1.16	3.47 x 10 <sup>5</sup>	4.04 x 10 <sup>-4</sup>
DFO-IgG C4 (H310A/H435Q)	1.04	3.39 x 10 <sup>5</sup>	3.53 x 10 <sup>-4</sup>
Fab C4	1.59	3.95 x 10 <sup>5</sup>	6.31 x 10 <sup>-4</sup>
DFO-Fab C4	1.36	3.86 x 10 <sup>5</sup>	5.27 x 10 <sup>-4</sup>

**Supplemental Table 3. Quality control of radiochemical purity after radiolabeling of the C4 ligands with <sup>89</sup>Zr. N = 2 experiments per C4 radioligand.**

	<sup>89</sup> Zr-IgG C4	<sup>89</sup> Zr-IgG C4 (H310A/H435Q)	<sup>89</sup> Zr-Fab C4
Radiochemical purity assessed by HPLC (%)	>96	>98	>96
Radiochemical purity assessed by iTLC (%)	>97	>95	>95

**Supplemental Table 4. Summary of the PET/CT imaging experiments performed in the human NSCLC xenograft models (H1975 and A549) with the anti-PD-L1 C4 radioligands.** For each experiment, activities were decay-corrected to the injection time. Data are presented as mean ± SD.

NSCLC tumor model	<sup>89</sup> Zr-labeled C4 ligand	Specific activity (MBq/nmol)	Injected activity (MBq)	Injected quantity (nmol)	Co-injected cold C4 ligand quantity (nmol)	Number of mice
H1975	IgG C4	11.6	4.3 ± 0.4	0.36 ± 0.03	/	6
	IgG C4	9.5	3.7 ± 0.4	0.40 ± 0.04	1.2 nmol	3
	IgG C4 (H310A/H435Q)	6.2	4.2 ± 0.2	0.66 ± 0.03	/	6
	IgG C4 (H310A/H435Q)	6.2	3.7 ± 0.2	0.60 ± 0.02	1.2 nmol	4
	Fab C4	7.5	4.0 ± 0.3	0.54 ± 0.03	/	6
	Fab C4	7.5	4.2 ± 0.3	0.57 ± 0.03	1.2 nmol	4
A549	IgG C4 (H310A/H435Q)	5.3	2.4 ± 0.2	0.45 ± 0.03	/	6
	Fab C4	2.0	2.6 ± 0.3	1.33 ± 0.13	/	5

**Supplemental Table 5. Biodistribution of the C4 radioligands in a PD-L1<sup>+</sup> human NSCLC xenograft model.** Female nude mice bearing subcutaneous PD-L1<sup>+</sup> H1975 xenografts were injected with the C4 radioligands, and PET/CT scans were acquired at selected times post-injection. Image-derived radioligand tissue uptake was expressed as percentage of injected dose per volume of tissue (%ID/cm<sup>3</sup>). Data are presented as mean ± SD.

<b><sup>89</sup>Zr-IgG C4 uptake (%ID/cm<sup>3</sup>)</b>						
<b>N = 6 mice</b>						
<b>Time post-injection</b>	<b>1 h</b>	<b>4 h</b>	<b>24 h</b>	<b>48 h</b>	<b>72 h</b>	<b>7 d</b>
Blood pool	18.10 ± 7.53	12.33 ± 1.24	7.97 ± 3.29	5.95 ± 2.48	5.43 ± 2.24	2.85 ± 1.48
Liver	12.66 ± 5.23	8.85 ± 0.45	6.20 ± 0.28	6.18 ± 0.35	5.78 ± 0.38	5.12 ± 0.36
Kidney	8.03 ± 3.32	5.83 ± 0.17	3.71 ± 0.53	2.96 ± 0.46	2.99 ± 1.24	1.71 ± 0.96
Spleen	8.17 ± 3.38	7.35 ± 0.18	5.48 ± 0.43	4.83 ± 0.27	4.60 ± 0.15	4.41 ± 0.19
H1975 tumor	1.36 ± 0.60	4.06 ± 0.47	4.53 ± 0.32	4.85 ± 0.61	4.15 ± 0.50	3.78 ± 0.24
Muscle	0.80 ± 0.35	1.02 ± 0.05	0.72 ± 0.08	0.59 ± 0.10	0.62 ± 0.09	0.58 ± 0.06
<b><sup>89</sup>Zr-IgG C4 (H310A/H435Q) uptake (%ID/cm<sup>3</sup>)</b>						
<b>N = 6 mice</b>						
<b>Time post-injection</b>	<b>1 h</b>	<b>4 h</b>	<b>24 h</b>	<b>48 h</b>	<b>72 h</b>	<b>7 d</b>
Blood pool	20.70 ± 0.90	12.19 ± 0.66	2.22 ± 1.22	0.96 ± 0.53	0.71 ± 0.39	0.58 ± 0.33
Liver	11.84 ± 1.06	12.39 ± 0.61	12.00 ± 0.51	10.55 ± 0.38	10.66 ± 0.63	10.26 ± 0.44
Kidney	9.05 ± 0.21	5.49 ± 0.44	1.56 ± 0.86	1.05 ± 0.58	0.85 ± 0.47	0.64 ± 0.35
Spleen	7.35 ± 0.78	6.72 ± 0.49	3.81 ± 0.58	3.09 ± 0.49	3.24 ± 1.77	2.78 ± 1.53
H1975 tumor	1.48 ± 0.15	3.92 ± 0.51	4.60 ± 0.39	3.48 ± 0.33	2.69 ± 0.27	1.69 ± 0.89
Muscle	0.72 ± 0.06	0.79 ± 0.06	0.49 ± 0.05	0.43 ± 0.06	0.39 ± 0.03	0.31 ± 0.16
<b><sup>89</sup>Zr-Fab C4 uptake (%ID/cm<sup>3</sup>)</b>						
<b>N = 6 mice</b>						
<b>Time post-injection</b>	<b>1 h</b>	<b>4 h</b>	<b>24 h</b>	<b>48 h</b>	<b>72 h</b>	
Blood pool	6.48 ± 2.74	0.86 ± 0.48	0.19 ± 0.11	0.12 ± 0.07	0.11 ± 0.06	
Liver	2.90 ± 0.31	1.46 ± 0.07	1.02 ± 0.13	0.90 ± 0.41	0.83 ± 0.38	
Kidney	69.57 ± 28.48	64.91 ± 4.50	40.08 ± 0.99	29.58 ± 13.40	22.76 ± 10.20	
H1975 tumor	1.06 ± 0.12	1.36 ± 0.11	0.79 ± 0.12	0.59 ± 0.26	0.50 ± 0.23	
Muscle	0.54 ± 0.08	0.22 ± 0.02	0.14 ± 0.02	0.13 ± 0.06	0.12 ± 0.05	

**Supplemental Table 6. Blocking experiments.** Female nude mice bearing subcutaneous PD-L1<sup>+</sup> H1975 xenografts were injected with the C4 radioligands, with or without co-injection of a 20X molar excess of non-radiolabeled C4 ligand. PET/CT scans were acquired at the optimal imaging time point for each C4 radioligand. Image-derived radioligand tissue uptake was expressed as percentage of injected dose per volume of tissue (%ID/cm<sup>3</sup>). Data are presented as mean ± SD.

	Radioligand uptake (%ID/cm <sup>3</sup> )					
	<sup>89</sup> Zr-IgG C4 48 h p.i.		<sup>89</sup> Zr-IgG C4 (H310A/H435Q) 24 h p.i.		<sup>89</sup> Zr-Fab C4 4 h p.i.	
	No blocking N = 6 mice	Blocking N = 3 mice	No blocking N = 6 mice	Blocking N = 4 mice	No blocking N = 6 mice	Blocking N = 4 mice
Blood pool	5.95 ± 2.48	6.20 ± 0.51	2.22 ± 1.22	2.90 ± 1.70	0.86 ± 0.48	0.75 ± 0.43
Liver	6.18 ± 0.35	6.76 ± 0.48	12.00 ± 0.51	11.51 ± 0.44	1.46 ± 0.07	1.40 ± 0.07
Kidney	2.96 ± 0.46	3.04 ± 0.23	1.56 ± 0.86	1.89 ± 1.09	64.91 ± 4.50	61.07 ± 1.96
Spleen	4.83 ± 0.27	4.55 ± 0.33	3.81 ± 0.58	4.25 ± 2.46	/	/
H1975 tumor	4.85 ± 0.61	2.17 ± 0.55	4.60 ± 0.39	2.43 ± 0.32	1.36 ± 0.11	0.73 ± 0.03
Muscle	0.59 ± 0.10	0.61 ± 0.09	0.49 ± 0.05	0.54 ± 0.05	0.22 ± 0.02	0.22 ± 0.02

**Supplemental Table 7. Human dosimetry of the C4 radioligands.** For each C4 radioligand, residence times (kBq.h.kBq<sup>-1</sup>) in main source organs (blood pool, liver, kidneys, spleen, remainder of the body) of individual mice were used as input in the IDAC-Dose software for extrapolation of human organ absorbed doses (mGy/MBq) and effective dose (mSv/MBq). Data are presented as mean ± SD. Organs with the highest absorbed dose estimates are indicated in bold.

Organ	Organ absorbed dose estimate (mGy/MBq)		
	<sup>89</sup> Zr-IgG C4	<sup>89</sup> Zr-IgG C4 (H310A/H435Q)	<sup>89</sup> Zr-Fab C4
<b>Adrenals</b>	0.61 ± 0.08	0.82 ± 0.12	<b>1.34 ± 0.26</b>
Brain	0.17 ± 0.03	0.10 ± 0.02	0.07 ± 0.03
Breast	0.25 ± 0.03	0.24 ± 0.02	0.12 ± 0.02
Colon wall	0.25 ± 0.03	0.21 ± 0.03	0.24 ± 0.05
Endosteum (bone surface)	0.22 ± 0.03	0.16 ± 0.03	0.12 ± 0.04
<b>Gallbladder wall</b>	<b>0.74 ± 0.06</b>	<b>1.14 ± 0.09</b>	0.59 ± 0.19
<b>Heart wall</b>	<b>1.09 ± 0.15</b>	<b>1.25 ± 0.16</b>	0.49 ± 0.17
<b>Kidneys</b>	0.74 ± 0.09	1.10 ± 0.12	<b>4.96 ± 0.92</b>
<b>Liver</b>	<b>0.92 ± 0.09</b>	<b>1.50 ± 0.16</b>	0.44 ± 0.08
Lungs	0.35 ± 0.05	0.36 ± 0.05	0.17 ± 0.03
Lymphatic nodes	0.30 ± 0.04	0.27 ± 0.03	0.23 ± 0.06
Muscle	0.22 ± 0.04	0.15 ± 0.03	0.13 ± 0.04
Esophagus	0.41 ± 0.04	0.43 ± 0.03	0.20 ± 0.02
Oral mucosa	0.19 ± 0.03	0.11 ± 0.02	0.08 ± 0.03
Ovaries	0.27 ± 0.04	0.16 ± 0.03	0.12 ± 0.04
<b>Pancreas</b>	0.47 ± 0.04	0.59 ± 0.04	<b>0.63 ± 0.22</b>
Prostate	0.23 ± 0.04	0.13 ± 0.02	0.10 ± 0.04
Red bone marrow	0.30 ± 0.04	0.25 ± 0.04	0.21 ± 0.05
Salivary glands	0.18 ± 0.03	0.11 ± 0.02	0.07 ± 0.03
Skin	0.15 ± 0.02	0.11 ± 0.02	0.08 ± 0.02
Small intestine wall	0.27 ± 0.04	0.24 ± 0.04	0.31 ± 0.08
Spleen	0.60 ± 0.07	0.50 ± 0.07	0.46 ± 0.10
Stomach wall	0.41 ± 0.04	0.48 ± 0.05	0.36 ± 0.10
Testes	0.18 ± 0.03	0.10 ± 0.02	0.07 ± 0.03
Thymus	0.29 ± 0.04	0.25 ± 0.04	0.13 ± 0.02
Thyroid	0.22 ± 0.03	0.15 ± 0.02	0.09 ± 0.03
Urinary bladder wall	0.21 ± 0.03	0.13 ± 0.02	0.10 ± 0.03
Uterus/cervix	0.26 ± 0.04	0.15 ± 0.03	0.12 ± 0.04
Effective dose (mSv/MBq)	0.34 ± 0.03	0.35 ± 0.02	0.26 ± 0.05

**Supplemental Table 8. Biodistribution of the C4 radioligands in PD-L1<sup>+</sup> and PD-L1<sup>-</sup> human NSCLC xenograft models.**

Female nude mice bearing subcutaneous PD-L1<sup>+</sup> H1975 xenografts or PD-L1<sup>-</sup> A549 xenografts were injected with the C4 radioligands, and PET/CT scans were acquired at selected times post-injection. Image-derived radioligand tissue uptake was expressed as percentage of injected dose per volume of tissue (%ID/cm<sup>3</sup>). Data are presented as mean ± SD.

<b><sup>89</sup>Zr-IgG C4 (H310A/H435Q) uptake (%ID/cm<sup>3</sup>)</b>						
<b>N = 6 mice per model</b>						
<b>Time post-injection</b>		<b>1 h</b>	<b>4 h</b>	<b>24 h</b>	<b>48 h</b>	<b>72 h</b>
Blood pool	H1975 model	20.70 ± 0.90	12.19 ± 0.66	2.22 ± 1.22	0.96 ± 0.53	0.71 ± 0.39
	A549 model	20.66 ± 0.90	11.20 ± 1.16	2.42 ± 1.33	1.11 ± 0.62	0.92 ± 0.51
Liver	H1975 model	11.84 ± 1.06	12.39 ± 0.61	12.00 ± 0.51	10.55 ± 0.38	10.66 ± 0.63
	A549 model	15.33 ± 0.68	19.19 ± 1.07	17.49 ± 0.93	13.12 ± 0.66	11.12 ± 1.20
Kidney	H1975 model	9.05 ± 0.21	5.49 ± 0.44	1.56 ± 0.86	1.05 ± 0.58	0.85 ± 0.47
	A549 model	9.20 ± 0.65	5.52 ± 0.41	1.42 ± 0.21	0.95 ± 0.53	0.99 ± 0.54
Spleen	H1975 model	7.35 ± 0.78	6.72 ± 0.49	3.81 ± 0.58	3.09 ± 0.49	3.24 ± 1.77
	A549 model	7.76 ± 0.56	7.00 ± 0.28	3.97 ± 0.29	2.75 ± 0.40	2.68 ± 0.37
Tumor	H1975 model	1.48 ± 0.15	3.92 ± 0.51	4.60 ± 0.39	3.48 ± 0.33	2.69 ± 0.27
	A549 model	0.93 ± 0.11	1.86 ± 0.17	2.27 ± 0.30	1.51 ± 0.33	1.34 ± 0.64
Muscle	H1975 model	0.72 ± 0.06	0.79 ± 0.06	0.49 ± 0.05	0.43 ± 0.06	0.39 ± 0.03
	A549 model	0.71 ± 0.06	0.77 ± 0.04	0.50 ± 0.07	0.40 ± 0.05	0.35 ± 0.16

<b><sup>89</sup>Zr-Fab C4 uptake (%ID/cm<sup>3</sup>)</b>						
<b>N = 5-6 mice per model</b>						
<b>Time post-injection</b>		<b>1 h</b>	<b>4 h</b>	<b>24 h</b>	<b>48 h</b>	<b>72 h</b>
Blood pool	H1975 model	6.48 ± 2.74	0.86 ± 0.48	0.19 ± 0.11	0.12 ± 0.07	0.11 ± 0.06
	A549 model	5.10 ± 1.11	1.45 ± 0.81	0.32 ± 0.18	0.16 ± 0.09	0.14 ± 0.08
Liver	H1975 model	2.90 ± 0.31	1.46 ± 0.07	1.02 ± 0.13	0.90 ± 0.41	0.83 ± 0.38
	A549 model	2.68 ± 0.39	1.76 ± 0.21	1.58 ± 0.17	1.33 ± 0.14	1.27 ± 0.18
Kidney	H1975 model	69.57 ± 28.48	64.91 ± 4.50	40.08 ± 0.99	29.58 ± 13.40	22.76 ± 10.20
	A549 model	76.44 ± 3.59	67.26 ± 5.36	46.97 ± 3.97	35.16 ± 3.88	27.58 ± 4.24
Tumor	H1975 model	1.06 ± 0.12	1.36 ± 0.11	0.79 ± 0.12	0.59 ± 0.26	0.50 ± 0.23
	A549 model	0.62 ± 0.06	0.65 ± 0.27	0.39 ± 0.17	0.30 ± 0.14	0.23 ± 0.12
Muscle	H1975 model	0.54 ± 0.08	0.22 ± 0.02	0.14 ± 0.02	0.13 ± 0.06	0.12 ± 0.05
	A549 model	0.39 ± 0.03	0.23 ± 0.10	0.16 ± 0.07	0.14 ± 0.06	0.10 ± 0.05